Validated coastal flood modeling at Imperial Beach, California: Comparing total water level, empirical and numerical overtopping methodologies.

T.W. Gallien[1]

Abstract

Flood extent field observations are used to evaluate the accuracy of static ('bathtub') and hydrodynamic coastal flood modeling methodologies. Static models rely on empirically calculated wave setup or runup and simply compare total water levels (TWL) to land elevation. The dynamic model resolves temporally variable overtopping rates, overland flow, urban features and storm system drainage. SWAN, a numerical wave model, transformed deep water buoy spectra to the nearshore. Static TWLs were calculated using SWAN output and an empirical runup model. Numerical (XBeach) and Empirical (EurOtop) overtopping models parameterized with survey data and SWAN bulk wave statistics estimated temporally variable overflow rates along representative transects for overland flow model input. XBeach model mode (hydrostatic, nonhydrostatic), boundary depth and random realizations significantly affected overtopping rates. Nonhydrostatic mode estimated order of magnitude larger overflow volumes suggesting the importance of incident waves, particularly in near threshold conditions. Boundary depth

Email address: tgallien@ucsd.edu (T.W. Gallien)
[1]Scripps Institution of Oceanography, University of California, San Diego

and random realizations varied overflow rates approximately fourfold. Field observations showed static TWL models performed poorly, maximum runup substantially overestimated flood extent and setup predicted no flooding. All dynamic models reasonably predicted flood extent despite significant overflow volume differences. Backshore topography and flow dynamics are important flood extent controls. Accurate near threshold coastal flood predictions require dynamic overland flow modeling parameterized with temporally variable overtopping estimates and site specific beach and backshore topography.

Keywords: wave overtopping, XBeach, coastal flooding, bathtub model, overwash, validation; nonlinear shallow water model, flood prediction, beach, field observation

1. Introduction

1.1. Background

Globally, coastal flooding represents a significant humanitarian and socioeconomic hazard, 20 million people live under current high tide levels and 200 million under storm tide levels (Nicholls, 2010). The recent IPCC report suggests global mean sea levels will rise 36-71 cm by 2100 under the RCP4.5 moderate emissions scenario (Church et al., 2013). Concerningly, mean higher high water (MHHW) and mean high water (MHW), peak levels that drive coastal flooding, show significant upward trends in many locations (Flick, 2002; Mawdsley et al., 2015). Relatively modest sea level rise (i.e., 0.50 m) will significantly increase flood frequencies (Hunter, 2012). For example, Sweet and Park (2014) show that 'tipping points', i.e., flooding over 0.5 m above MHHW levels will be reached by 2050, while Tebaldi et al. (2012) suggest that the 100 year coastal flood will become annual to decadal events for much of the United States.

Coastal flood vulnerability is evaluated using two modeling methodologies; static (also known as bathtub, equilibrium or planar surface projection models), and hydrodynamic models (e.g., BreZo, DIVAST, TELEMAC-2D, TUFLOW) that solve the equations of mass and momentum. Static methods simply compare water and land elevations and assume that flooding occurs instantaneously when water levels exceed backshore elevations. Static models (e.g., Heberger et al., 2009; Climate Central, 2015; NOAA, 2015) are widely used to assess regional sea level rise vulnerability and have been shown to substantially overpredict coastal flooding in low elevation backshores(Bernatchez et al., 2011; Gallien et al., 2011; Gallien, 2014). Two-dimensional (2D) hydro-

dynamic models accurately simulate long wave dynamics and overland flow (e.g., Bates et al., 2005; Brown et al., 2007; Purvis et al., 2008; Dawson et al., 2009; Knowles, 2009; Martinelli et al., 2010; Smith et al., 2012; Wadey et al., 2012). However, temporally and spatially variable overtopping, fundamental to accurate coastal flood prediction, are rarely included in hydrodynamic flooding models. Overtopping flows are a significant deficiency in coastal flood modeling efforts (Hubbard and Dodd, 2002; Hunt, 2005; Brown et al., 2007), and prioritized as a critical future research area (Wadey et al., 2012).

A simplistic method for representing overtopping flows uses a calculated total water level (TWL) based on Stockdon et al. (2006) $R_{2\%}$ (e.g., FEMA, 2004; Heberger et al., 2009) or maximum water level output from numerical models such as XBeach (e.g., Barnard, 2014). TWL models are applied using a static (bathtub) method, projecting the maximum water level over the backshore and suffers identical deficiencies as typical static modeling, significantly overpredicting backshore flooding (Bates et al., 2005; Gallien, 2014). Few studies have attempted to resolve temporally and spatially variable overtopping flows and fewer still incorporate validation data. Laudier et al. (2011) investigated beach overtopping and lagoon filling in Central California and suggested that empirical overtopping models overestimated total overtopped volume. Gallien (2014) used empirical overtopping estimates as source point input into an overland flow solver and showed good agreement with validation data, though some overprediction was observed. Cheung et al. (2003) and Lynett et al. (2010) presented numerical overtopping models along with qualitative validation data (e.g., high water marks or levee damage), however in the case of Lynett et al. (2010), empirical and numerical

estimates differed by an order of magnitude. Le Roy et al. (2014) coupled nearshore wave and phase resolving nonlinear shallow water (NLSW) models to hindcast overtopping flooding, however variable quality high water marks supported only qualitative validation. Numerous studies show the critical need for field validation data (e.g., Battjes and Gerritsen, 2002; Poulter and Halpin, 2008; Reeve et al., 2008; Anselme et al., 2011; Gallien et al., 2012).

XBeach (Roelvink, 2009) is a process based flow and sediment transport model that considers infragravity and incident wave forcing. XBeach solves a time dependent wave action balance that forces a Generalized Lagrangian Mean (GLM) formulation of the nonlinear shallow water equations (Roelvink, 2009). A one-layer, nonhydrostatic pressure correction (Zijlema and Stelling, 2008) enables short wave surface elevation variation. For a complete model description see Roelvink (2009) and Smit et al. (2010). XBeach has been used primarily to model erosion and overwash during storm events (e.g., Roelvink, 2009; McCall et al., 2010; Splinter and Palmsten, 2012; McCall, 2013). Here, uncalibrated XBeach is used to numerically estimate temporally variable overtopping volumes on a sandy beach during a winter storm event. Wave, water level and flooding observations and modeling are described in Section 2. Results are presented in Section 3. Modeling methodology, boundary conditions and site specific data discussions (Section 4) are followed by a summary (Section 5).

2. Methods

2.1. Site Description

Imperial Beach, California is a low-lying southern California coastal community located between San Diego and the US-Mexico border. The southernmost portion of the city, Figure 1C, is a sand spit backed by the Tijuana Estuary that frequently floods. In September and October, 2012 344,000 m^3 of sand were placed on the beach from Cortez Avenue south adding approximately 60 m of subaerial beach. The nourishment profile steepened, retreated and developed wave cut crowns (Ludka and Guza, 2015).

2.2. Flood Event Description

On January 30, 2014 winter storm waves (H_s ~1.8 m, T_p ~14 s, D_p ~ 280°) coinciding with a spring high tide, 2.1 m North American Vertical Datum of 1988 (NAVD88), overtopped Imperial Beach's southern reach, flooding Cortez, Descanso and Seacoast Drive. The field team arrived at 14:30 coordinated universal time (UTC) and observed overtopping and minor flooding. Overtopping peaked around 16:00 UTC and occurred intermittently until approximately 18:15 UTC. A hand dolly fitted with a Real Time Kinematic (RTK) receiver mapped the maximum flood extent.

2.3. Digital Elevation Model Topographic and Bathymetric Datasets

A digital terrain model (DTM) from approximately 33 km offshore and 500 m landward of the beach was constructed in World Geodetic System 1984 (WGS84) and NAVD88 m (Figure 1) using offshore bathymetry from NOAA Geophysical Data Center (Carignan, 2012) and bare earth California Coastal Conservancy topography from NOAA digital Coast (http://coast.noaa.gov/dataviewer).

Priority	Location	Description	Source	Date	Resolution (m)	VRMSE (cm)
1	Beach crest	Dolly survey	Scripps	01-30-14	0.8[1]	2
2	Upper beach	ATV survey	Scripps	01-30-14	0.6[2]	3
3	Beach to -8 m	ATV, dolly, jet ski	Scripps	01-14-14	0.8[3]	3
4	Backbeach	LiDAR DSM	Scripps	04-08	2	10
5	Land/Estuary	Bare earth DEM	CA Coastal Cons.	10-09 to 08-11	1	10
6	Offshore	1/3 Arc Second DEM	NOAA NDGC	various	1-10	10-100

Table 1: Geospatial data. Resolution given is point spacing along crest line[1], 5 m transects[2] and 100 m transects[3]

The bare earth digital elevation model (DEM) exhibits a highly smoothed landward sloping surface inconsistent with the site (Figure 2). An alternate LiDAR digital surface model (DSM) that did not remove structures was consistent with the observed back beach region. DSM elevation data between houses were used to supplant incorrect bare earth DEM elevations. Beach crest elevations were surveyed immediately before high tide, comprehensive beach topography was surveyed at the following low tide. Nearshore bathymetry from 0 to -8 m NAVD88 m was surveyed two weeks prior to the overtopping event. Beach topography was blended with nearshore bathymetry, bare earth topographic data (NOAA, 2014a) and offshore bathymetry. Table 1 shows the data sources, in order of priority, used to construct the DTM.

2.4. Wave Modeling

Six minute water levels were obtained from the nearest open coast tide gauge, La Jolla 9410230, approximately 40 km north and applied as offshore boundary conditions for all models. Deep water boundary condition half-hourly frequency directional spectra (CDIP buoy 191, http://cdip.ucsd.edu) were calculated using the maximum entropy method (64 frequency, 360 directional bins) and propagated shoreward using SWAN (Booij et al., 1999).

The 33 x 20 km (660 x 400) simulation domain, gridded at ∼50 m spacing, was carefully chosen to preserve wave properties in the region of interest, i.e. boundary shadowing and grid resolution effects were negligible. An eight hour non-stationary simulation (1100-1900 UTC) output significant wave height (H_s), peak period (T_p), peak direction (D_p) and directional spread (σ_e) at 6 minute intervals at 40 m, 10 m the slope toe (∼-1 m NAVD88) along three representative cross-shore transects (Figure 3). The first hour of output was discarded.

2.5. TWL Estimates

Total water levels were estimated using Stockdon et al. (2006) setup $\langle\overline{\eta}\rangle$ and runup, $R_{2\%}$,

$$\langle\overline{\eta}\rangle = 0.35\beta(H_0L_0)^{0.5} \tag{1}$$

$$R_{2\%} = 1.1\left(0.35\beta(H_0L_0)^{0.5} + \frac{[H_0L_0(0.563\beta^2 + 0.004)]^{0.5}}{2}\right) \tag{2}$$

where β is the slope, H_0 is the deep water significant wave height, L_0 is the deep water wave length. SWAN significant wave height estimates in 40 m depth were linearly reverse shoaled for calculating Stockdon TWLs.

2.6. Dynamic water level and overtopping estimates

Maximum wave runup elevation and overtopping volumes were estimated over a seven hour period (1200-1900 UTC) using EurOtop (Pullen, 2007) and XBeach (Roelvink, 2009). EurOtop was developed for dike structures and relies on bulk wave parameters and beach geometry to estimate average

overtopping rates. Although EurOtop is intended for runup and overtopping of structures it has been used to estimate beach and dune overtopping volumes (e.g., Martinelli et al., 2010; Laudier et al., 2011; Gallien, 2014). The probabilistic EurOtop formulation for $\xi_{m-1,0} < 5$ is,

$$\begin{aligned} \frac{q}{\sqrt{gH_{m0}^3}} &= \min(a, b) \\ \mathrm{a} &= \frac{0.067}{\sqrt{\tan\alpha}}\gamma_b\,\xi_{m-1,0}\exp\left(-4.75\frac{R_c}{\xi_{m-1,0}H_{mo}\gamma_b\gamma_f\gamma_\beta\gamma_v}\right) \\ \mathrm{b} &= 0.2\exp\left(-2.6\frac{R_c}{H_{m0}\gamma_f\gamma_\beta}\right) \end{aligned} \tag{3}$$

where q is the mean overtopping rate per unit length, g represents gravity, α is slope angle, R_c is the freeboard, H_{m0} is the significant wave height at the structure toe, γ_b is the berm influence factor, γ_f is the roughness influence factor, γ_β is the oblique wave attack factor, γ_v is the vertical wall influence factor (Pullen, 2007). All reduction parameters were assumed to be unity. The TAW (2002) formulation relies on a breaker parameter $\xi_{m-1,0}$ that characterizes the wave breaking condition (i.e., breaking, non-breaking) and is given as,

$$\xi_{m-1,0} = \frac{\tan\alpha}{\sqrt{\frac{H_{m0}}{L_{m-1,0}}}} \tag{4}$$

where $L_{m-1,0} = gT_{m-1,0}^2/2\pi$ and $T_{m-1,0} \approx T_p/1.1$ (Pullen, 2007). Wave overtopping volumes were estimated using $T_{m-1,0}$ calculated from 30 minute buoy data, six minute SWAN significant wave height output at the slope toe and beach topography from the DTM.

Although Stockdon calculates runup and EurOtop estimates overtopping, overtopping is a function of runup and would presumably include identical

physical dependencies. The dependency in Stockdon is the product of $H_0 L_0$ while EurOtop (Eqt. 4) depends on the dividend $H_{m0}/L_{m-1,0}$.

XBeach was run in one-dimensional (1D) profiles in hydrostatic and non-hydrostatic mode along three transects. Spatially variable 1D grids were optimized using the XBeach Matlab toolbox 'xb_grid_xgrid'. Hydrostatic gridding resulted in approximately 120 and 270 cells for offshore XBeach boundary conditions in 10 m and 40 m depths, respectively. Nonhydrostatic gridding resulted in approximately 600 and 2900 cells for the 10 and 40 m boundaries, respectively. SWAN bulk wave parameters and La Jolla water levels were used as offshore boundary conditions. Sediment transport and morphology were set to 0 (off). Recent studies impose XBeach boundaries in relatively shallow, 8-15m, depths (e.g., Barnard, 2014; Stockdon et al., 2014). In the present case, ∼40 m satisfies the ratio of group celerity to wave celerity (n∼0.8, kd∼1) recommended on the XBeach forum (McCall, 2013). Ten XBeach realizations using 10 and 40 m SWAN outputs (H_s, T_p, σ_e) were run in both hydro- and non-hydrostatic modes along three transects (120 total simulations). Wave overtopping volumes were estimated at 1 Hz from water height and velocities immediately shoreward of the maximum beach elevation (arrow, Figure 4C) for each transect. Hydrostatic run times were approximately 90 and 140 seconds for 10 and 40 m. Nonhydrostatic run times were approximately 600 and 3600 seconds for 10 and 40 m, respectively.

2.7. Flood Modeling

Overland flow and drainage from the storm water system was modeled using BreZo, a two-dimensional Godunov type finite volume model that solves the nonlinear shallow water equations. A constrained Delaunay triangulation

was generated using Triangle (Shewchuk, 1996) consisting of 8234 triangles represented the 1200 m x 380 m domain along Seacoast Drive. A spatially variable mesh, gradating from ∼25 m offshore to ∼3 m along beaches and roads where flooding occurred. A minimum of three cells across were used to resolve street flows. Wave overtopping volumes were introduced to the overland flow model at multiple locations to consider source point number, distribution and position effects.

Surface streets are gravity drained into the estuary via the storm water system and are represented by point sinks in the overland flow model using a weir equation;

$$Q_{ss} = \frac{2}{3} C_d \left(\frac{2}{3} g\right)^{1/2} L H^{3/2} \tag{5}$$

where Q_{ss} represents flow into the storm sewer, C_d is the coefficient of discharge, L is the drain opening width and H is the water depth.

Flood modeling was performed in serial on a Dell T3600 workstation with an Intel quad core 3.6GHz processor. A 7 hour simulation, resolving the rising, peak and ebbing tide required approximately 5 minutes of CPU time. A 0.2 s time step satisfied the Courant-Friedrichs-Levy (CFL) criterion. The model was first applied using a tidal boundary condition to consider the possibility of ocean or bay-side tidal flooding. Consistent with observations, no tidal flooding occurred. All flooding was caused exclusively by ocean-side overtopping.

2.8. Fit Measures

Three fit metrics describe the goodness-of-fit between predicted and observed flood extents. The coefficient of areal correspondence, F_A (Taylor,

1977), shows the agreement between prediction and observation and is defined as the intersection of predicted and observed flood extents divided by the union of the predicted and observed flood extent,

$$F_A = \frac{E_P \cap E_O}{E_P \cup E_O} \tag{6}$$

where E_O and E_P represent the observed and predicted flood extent, respectively. Perfect agreement would result in $F_A = 1$. Underprediction, F_{UP}, is characterized by the fraction of flooded area observed, but not predicted.

$$F_{UP} = \frac{E_O - E_P \cap E_O}{E_P \cup E_O} \tag{7}$$

$F_{UP} = 0$ corresponds to no underprediction. Lastly, overprediction, F_{OP}, characterizes the fraction of flooded area predicted but not observed.

$$F_{OP} = \frac{E_P - E_P \cap E_O}{E_P \cup E_O} \tag{8}$$

and $F_{OP} = 0$ corresponds to no overprediction. Superior models will maximize F_A and minimize both F_{UP} and F_{OP}.

3. Results

3.1. Runup and overtopping

Table 2 shows Stockdon $R_{2\%}$ runup and average maximum onshore water levels, the maximum free surface elevation measured at the beach crest, for all XBeach realizations. Slope dependency is observed in both empirical and numerical results, maximum runup increases with beach foreshore steepness but is considerably stronger in Stockdon. Stockdon $R_{2\%}$ varies by 60 cm

Transect	β	z_{max}	$R_{2\%}$	10 m hydro	10 m nonhydro	40 m hydro	40 m nonhydro
3	0.117	4.34	4.54	4.49(0.06)	4.79(0.10)	4.12(0.18)	4.65(0.04)
6	0.096	4.24	4.19	4.45(0.07)	4.71(0.18)	4.09(0.19)	4.51(0.07)
9	0.132	4.52	4.79	4.60(0.05)	4.81(0.11)	4.15(0.26)	4.67(0.06)

Table 2: Transect data, Stockdon runup and XBeach average maximum onshore water level results. All dimension in meters, except slope, β (non-dimensional). z_{max} is the maximum beach elevation. Standard deviations are shown in parentheses.

across the three transects while XBeach average maximum onshore water level elevations vary less than 16 cm. Each XBeach model considers 10 realizations, maximum water level estimates for all realizations and transects (120 total) varied from ∼3.8 to 5 m. Model mode (i.e., hydrostatic, nonhydrostatic) and boundary depth significantly effect XBeach water level estimates (Table 2). Across all transects, hydrostatic models estimated substantially lower (21-53 cm) runup than corresponding nonhydrostatic results. Lower average maximum water levels (14-45 cm) were observed using the deeper 40 m boundary.

XBeach boundary depth (10 or 40 m) and modeling mode (hydrostatic or nonhydrostatic) significantly affect overtopping estimates. Nonhydrostatic modeling increased transect overtopping rates and volumes (Table 3, Figure 5) and predicted overtopping for all realizations (60 total). Hydrostatic modeling predicted overtopping for nearly all 10 m realizations (Figure 5, white bands, dashed blue lines) but only 16% (5/30) of the 40 m realizations (Figure 5, grey bands, blue asterisks).

XBeach predicts impulsive overtopping rates while EurOtop predicts average overtopping rates (Figure 6), accordingly XBeach predicts substantially

Model	Mode	Depth (m)	Transect	q_{max} l/s/m	Q_{tot} (l/m)	V_{total} (m^3)	T_{ot} (s)	Q_{avg} (l/m/s)
		0	3	25.45	162,180	12,164	19,080	8.5
EurOtop		0	6	11.52	64,900	3,894	14,760	4.4
		0	9	32.46	193,860	18,147	19,440	10.0
		10	3	433	4,531(2,380)	387	57.4(14.4)	76.4(32.2)
XBeach	Hydrostatic	10	6	600	12,827(2,908)	673	282(49)	46.3(10.6)
		10	9	158	1,263(1,311)	97	20(12)	50.6(31.0)
		10	3	2,393	35,171(7,626)	2,901	337(28)	102(16)
XBeach	Nonhydrostatic	10	6	1,866	34,124(5,470)	2,028	361(41)	95(15)
		10	9	1,043	6,042(3,126)	573	63(24)	97(38)
		40	3	$*$	$*$	$*$	$*$	$*$
XBeach	Hydrostatic	40	6	$*$	$*$	$*$	$*$	$*$
		40	9	$*$	$*$	$*$	$*$	$*$
		40	3	831	8,595(6,222)	645	113(19)	78(35.5)
XBeach	Nonhydrostatic	40	6	685	7,471(3,802)	439	192(66)	37.5(11.1)
		40	9	290	2,142(1,459)	204	54.4(21.5)	364(13.6)

Table 3: Overtopping model results. EurOtop results are deterministic. Each XBeach model was run 10 times for each transect, the mean and standard deviations (in parenthesis) are shown. Overtopping time (T_{ot}) is considered for flows over 1 l/s/m. q_{max} and V_{total} are runs nearest to the mean. V_{total} is scaled by the representative reach length of each transect. $*$indicates zero or insignificant overtopping.

higher maximum overtopping rates (q_{max}) while EurOtop predicts orders of magnitude higher overtopped (Q_{tot}) and total (V_{total}) volumes. For example, on transect 3 EurOtop predicts a maximum rate of 25.5 l/s/m and a total overtopped volume of 1.6 x 10^5 l/m, nonhydrostatic 40 m XBeach predicts maximum rates and volumes of 831 l/s/m and 8,595 l/m.

EurOtop's exponential formulation always predicts overtopping, if flows over 1 l/s/m are considered, EurOtop predicts overtopping flows for over four hours while XBeach only predicts 1-5 minutes total overtopping time (Figure 6). If average overtopping rates are considered i.e., total overtopped volume (Q_{tot}) divided by the overtopping time (T_{ot}) order of magnitude differences are observed. EurOtop and nonhydrostatic XBeach realizations at 10 and 40 m depths nearest to the mean overtopping rate were chosen as input to the hydrodynamic flood model.

3.2. Static and Hydrodynamic Flood Modeling

Five total flood models are considered (Table 4); two static water levels, Stockdon setup and $R_{2\%}$ (Figure 7A), and three hydrodynamic models using EurOtop, XBeach 10 m nonhydrostatic, and XBeach 40 m nonhydrostatic overtopping estimates (Figures 7B-D, respectively). Static TWL flood prediction is poor; Stockdon setup (not shown) predicts no flooding ($F_A = 0$, $F_{UP} = 1$) while $R_{2\%}$ extensively overpredicts ($F_A = 0.13$, $F_{OP} = 0.87$). Flood models parameterized with nonhydrostatic 40 m XBeach (Figure 7D) were most consistent with areal extent ($F_A = 0.71$), flood arrival time and qualitative depth observations. From an areal extent perspective, all hydrodynamic models perform similarly ($F_A \sim 0.7$) despite order of magnitude differences in overtopped volume inputs. However, flow characteristics differ substan-

Model	F_A	F_{OP}	F_{UP}	h_{avg}	h_{max}	h_{Cortez}
Stockdon $R_{2\%}$	0.13	0.87	0	-	-	-
Stockdon SU	0	0	1	-	-	-
EurOtop	0.64	0.34	0.02	9.5	27.3	2.4
10 m XBeach	0.67	0.29	0.04	10.9	25.1	9.9
40 m XBeach	0.71	0.15	0.14	6.9	18.9	5.3

Table 4: Flood models and statistics. All heights are in centimeters.

tially. EurOtop overtopping is a long, slow filling event, maximum water levels near the beach are 2.4 cm (Table 4, h_{Cortez}) compared to higher levels, 5-10 cm, for impulsive (XBeach) overtopping. Flow vector analysis suggests constant low level EurOtop flows are constrained by the curb, spread along gutters and discharge through the storm drains (Figure 7B). Conversely, in impulsive flooding events water flows down Descanso and Cortez streets and surges across the curb into the estuary.

3.3. Overtopping Input Locations and Spacing

Wave overtopping volume time series are input to the overland flow model as source points at various long and cross-shore locations. In hard structure flood modeling, grid cells or mesh edges are aligned with infrastructure (i.e., sea walls) and overtopping volumes are introduced along these features (e.g., Prime, 2015). Beaches, however, include fine scale, sub-meter topography (e.g., cusps, scarp), representing meshing challenges similar to those reported by Tsubaki and Fujita (2010) and Gallien et al. (2011). A computationally efficient mesh prohibits exact representation of the beach crest, some mesh cells will interpolate across the high elevation crest. Flow vector analysis shows grid cells that interpolate across the high elevation feature may in-

Trial	Δlongshore	cross-shore location	points	F_A	F_{OP}	F_{UP}	A (m^2)	h_{avg}	h_{max}
1	5	landward crest	46	0.60	0.09	0.31	2,007	5.56(4.02)	17.9
2	5	2 grid cells landward	46	0.71	0.15	0.14	2,674	6.90(3.74)	18.9
3	5	between crest/trough	46	0.71	0.15	0.14	2,677	6.90(3.76)	19.0
4	5	trough	46	0.71	0.15	0.14	2,723	7.38(3.83)	19.1
5	10	between crest/trough	23	0.71	0.15	0.14	2,675	6.78(3.85)	19.3
6	15	between crest/trough	15	0.71	0.15	0.14	2,689	6.97(3.88)	19.2
7	20	between crest/trough	11	0.71	0.15	0.14	2,672	6.78(3.82)	19.2
8	30	between crest/trough	8	0.71	0.15	0.14	2,693	6.89(4.03)	19.9
9	40	between crest/trough	5	0.71	0.15	0.14	2,717	7.54(3.84)	18.7
10	~ 80	between crest/trough	3	0.69	0.23	0.08	3,201	10.1(5.29)	22.3
11	~ 80	trough	3	0.65	0.31	0.04	3,672	14.4(9.30)	63.0

Table 5: Overtopping Input Points Summary

correctly slope and route overtopped water seaward. Input point cross-shore placement relative to beach crest, mesh edges and cell slope become important. Various cross-shore input locations are considered (Table 5, Trials 1-4); aligned immediately landward the DTM maximum beach elevation contour, two grid cells landward of the maximum beach elevation, along a line approximately halfway between the maximum beach elevation and low elevation contour landward of the crest but seaward of the urbanization and finally, the low elevation beach contour. All trials produced nearly identical results except when input points were aligned with the DTM maximum beach elevation contour (Trial 1).

4. Discussion

Backshore flooding results from dynamic wave runup and overtopping processes. Temporally variable overtopping volume models were superior to

TWL methods. All static models are incapable of resolving dynamic overtopping flows. Simple Stockdon $R_{2\%}$ TWL models substantially overpredicted flood extent. Conversely, setup TWL predicted no backshore flooding. Continued reliance on static methods and corresponding poor prediction undermines coastal flood risk management efforts.

Interestingly, flood extents were similar for all dynamic overtopping models despite orders of magnitude difference in overtopped volume, suggesting that backshore topography and flow dynamics are primary flood extent controls.

Typically, XBeach is applied in a single deterministic run and offshore boundaries are imposed at instrumentation locations (e.g., Stockdon et al., 2014) or set depths (e.g., Barnard, 2014). Random realizations of otherwise identical XBeach runs yielded significant variation in overtopping estimates, particularly when runup elevations are similar to maximum beach elevations. Although relative standard deviations decreased with increasing freeboard exceedance and subsequent overtopping events, overflow discrepancies may result in fundamentally different flooding predictions, particularly in areas with estuary side sea walls that retain overtopped volumes (e.g., Gallien, 2014). Alternative offshore boundaries (10 and 40 m) varied average maximum water levels by 14-45 cm and overtopping estimates approximately fourfold, suggesting that infragravity energy generated at the XBeach boundary varies significantly with boundary depth.

Long and cross-shore input spacings must be considered for accurate flood predictions. Input spacings should be distributed along the beach, sufficiently seaward of urban features and landward of beach crest such that overtopped

water correctly routes across the beach surface (Table 5, Trials 2-9). In this case, longshore spacings of 30 m or less appropriately routed water across local topographic depressions and into the backshore. Cross-shore inputs coinciding with seaward sloping grid cells incorrectly routed overtopped volume and should be avoided (Table 5, Trial 1). Sparse longshore (in this case, 80 m) or excessively landward input points (Table 5, Trial 11) caused significant overprediction.

Generally, bare earth LiDAR based DTMs are recommended for routing overland flows (Sanders, 2007). However, in steep and rapidly variable terrain common to urbanized sand spits, structure removal may oversmooth high backbeach elevations. Figure 2 shows the difference between the bare earth DTM and a LIDAR DSM, differences of $\sim$2 m are observed between the two datasets between buildings. This highlights the critical site knowledge required to accurately model rapidly variable, urbanized backshore terrain.

5. Conclusions

A nested modeling methodology is used to predict wave overtopping flooding. SWAN transformed offshore buoy data to the nearshore where XBeach estimated wave overtopping volumes as input to a a nonlinear shallow water solver for backshore flood prediction. Model results are compared to traditional static TWL flood modeling. Field observations show TWL methods perform poorly, resulting in extensive over or under-prediction. All temporally variable overtopping models results were superior to static methods.

XBeach is often applied in a single deterministic run (e.g., Barnard, 2014; Stockdon et al., 2014), however random realizations showed significant runup

and overtopping variability within each group of 10 runs. Boundary depth also significantly affected runup and overtopping rates. Both random realizations and appropriate offshore boundary depths for expected wave numbers must be considered.

Accurate beach and back-beach topographic characterization are crucial in rapidly variable, densely built coastal areas. Local beach depressions retained and infiltrated overtopped flows. The bare earth DEM oversmoothed high elevations where structures were removed. In this case, terrain changes could be observed in Google Earth and alternative LiDAR data was available to supplant the problematic region. Accurate urban coastal flood modeling often requires site specific knowledge and topographic data.

Wave overtopping field observations are exceedingly rare and validation data paucity inhibits accurate urban coastal flood modeling and prediction. This study benefits from flood extent observations; however, depth, velocity field and overflow measurements are needed to rigorously validate impulsively driven overtopping flows and advance coastal flood modeling.

6. Acknowledgments

This work was supported by the University of California, San Diego Chancellor's Fellowship, California Department of Parks and Recreation, Division of Boating and Waterways (program manager R. Flick) and the United States Army Corps of Engineers. Brian Woodward, Kent Smith, Dennis Darnell, Bill Boyd and Rob Grenzeback collected beach and bathymetry data used in this work.

References

Anselme, B., Durand, P., Thomas, Y.F., Nicolae-Lerma, A., 2011. Storm extreme levels and coastal flood hazards: A parametric approach on the French coast of Langunedoc (district of Leucate). Comptes Rendus Geoscience 343, 677-690.

Battjes, J.A. and Gerritsen, H., 2002. Coastal modelling for flood defence. Philosophical Transactions of the Royal Society A 360, 1461-1475.

Barnard, P.L., van Ormondt, M., Erickson, L.H., Eshleman, J., Hapke, C., Ruggiero, P., Adams, P.N., Foxgrover, A.C., 2014. Development of the Coastal Storm Modeling System (CoSMoS) for predicting the impact of storms on high-energy active-margin coasts. Natural Hazards, 74(2), 1095-1125.

Bates, P.D., Dawson, R.J., Hall, J.W., Horritt, M.S., Nicholls, R.J.,Wicks, J., Hassan, M.A.A.M., 2005. Simplified two-dimensional numerical modelling of coastal flooding and example applications. Coastal Engineering 52(9), 793-810.

Bernatchez, P., Fraser, C., Lefaivre, D., Dugas, S., 2011. Integrating anthropogenic factors, geomorphological indicators and local knowledge in the analysis of coastal flooding and erosion hazards. Ocean and Coastal Management, 53, 621-632.

Booij, N., Ris, R. C., Holthuijsen, L. H., 1999. A thirdgeneration wave model for coastal regions: 1. Model description and validation. Journal of Geophysical Research: Oceans (19782012), 104(C4), 7649-7666.

Brown, J.D., Spencer, T., Moeller, I., 2007. Modeling storm surge flooding of an urban area with particular reference to modeling uncertainties: A case study of Canvey Island, United Kingdom. Water Resour Res. 43(W06402), doi:10.1029/2005WR004597.

Carignan, K.S., L.A. Taylor, B.W. Eakins, D.Z. Friday, P.R. Grothe, and M. Love, 2012. Digital Elevation Models of San Diego, California: Procedures, Data Sources and Analysis, NOAA National Geophysical Data Center technical report, Boulder, CO, 32 pp.

Cheung, K.F., Phadke, A.C., Wei, Y., Rojas, R., Douyere, Y.J.M., Martino, C.D., Houston, S.H., Liu, P.L.F., Lynett, P.J., Dodd, N., Liao, S., Nakazaki, E., 2003. Modeling of storm induced coastal flooding for emergency management. Ocean Engineering 30, 1353-1386.

Church, J.A., Clark, P.U., Cazenave, A., Gregory, J.M., Jevrejeva, S., Levermann, A., Merrifield, M.A., Milne, G.A., Nerem, R.S., Nunn, P.D., Payne, A.J., Pfeffer, W.T., Stammer, D., and Unnikrishnan, A.S.: Sea level change. In: Climate Change 2013: The Physical Science Basis, Contribution of Working Group I to the Fifth Assessment Report of the Intergovernmental Panel on Climate Change, edited by: Stocker, T.F., Qin, D., Plattner, G.-K., Tignor, M., Allen, S.K., Boschung, J., Nauels, A., Xia, Y., Bex, V., and Midgley, P.M. (eds), Cambridge University Press, Cambridge, UK, New York, NY, USA, 11371216, 2013.

Climate Central. Surging Seas, Sea level rise analysis by Climate Central. Accessed May 5, 2015 at `http://sealevel.climatecentral.org/`

Dawson R.J., Dickson M.E., Nicholls R.J., Hall J.W., Walkden M.J.A., Stansby P., Mokrech M., Richards J., Zhou J., Milligan J., Jordan A., Pearson S., Rees J., Bates P., Koukoulas S., Watkinson A., 2009. Integrated analysis of risks of coastal flooding and cliff erosion under scenarios of long term change. Climatic Change 95(1-2), 249-288.

Federal Emergency Management Agency (FEMA), 2004. Guidelines and Specifications for Flood Hazard Mapping Partners Appendix D. Final Draft Guidelines for Coastal Flood Hazard Analysis and Mapping for the Pacific Coast of the United States. Available online at `http://www.fema.gov/library/viewRecord.do?id=2188`.

Flick, R., Murray, J., Ewing, L. 2003. Trends in United States Tidal Datum Statistics and Tide Range. J. Waterway, Port, Coastal, Ocean Eng., 129(4), 155164.

Gallien, T.W., Schubert, J.E, and Sanders, B.F., 2011. Predicting tidal flooding of urbanized embayments: A modeling framework and data requirements. Coastal Engineering, 58(6), 567-577.

Gallien, T.W., Barnard, P., van Ormondt, M., Foxgrover, A., Sanders, B.F., 2012. A Parcel-scale coastal flood forecasting prototype for a Southern California urbanized embayment. Journal of Coastal Research, 31, 47-60.

Gallien, T.W., Sanders, B.F., Flick, R.E., 2014. Urban coastal flood prediction: Integrating wave overtopping, flood defenses and drainage. Coastal Engineering 91, 18-28.

Guza, R.T. and Feddersen, F., 2012. Effect of wave frequency and directional spread on shoreline runup. Geophysical Research Letters, 39, L11607, 5 pp.

Heberger, M., Cooley, H., Herrera, P., Gleick, P.H., Moore, E., 2009. The impacts of sea-level rise on the California coast. Sacramento, California Climate Change Center.

Holthuijsen, L.H., Booij, N., Herbers, T.H.C., 1989. A prediction model for stationary, short-crested waves in shallow water with ambient currents. Coastal Engineering 13, 2354.

Hubbard, M.E., Dodd, N., 2002. A 2D numerical model of wave run-up and overtopping. Coastal Engineering 47, 1-26.

Hunt, J.C.R., 2005. Inland and coastal flooding: developments in prediction and prevention. Philosophical Transactions of the Royal Society A 363, 1475-1491.

Hunter, J., 2012. A simple technique for estimating an allowance for uncertain sea-level rise. Climatic Change 113, 239-252.

Knowles, N., 2009. Potential inundation due to rising sea levels in the San Francisco Bay Region. Sacramento, California Climate Change Center.

Laudier, N.A., Thornton, E.B., MacMahan, J., 2011. Measured and modeled wave overtopping on a natural beach. Coastal Engineering 58, 815-825.

Le Roy, S., Pedreros, R., Andr, C., Paris, F., Lecacheux, S., Marche, F., Vinchon, C., 2014. Coastal flooding of urban areas by overtopping: dynamic

modelling application to the Johanna storm (2008) in Gâvres (France). Natural Hazards and Earth System Sciences Discussions, 2(8), 4947-4985.

Ludka, B.C., Guza, R.T., OReilly, W.C. (2015), Observations of Four Nourished Beaches, in Coastal Sediments 2015, San Diego, CA.

Lynett, P.J., Melby, J.A., Kim, D.H., 2010. An application of Boussinesq modeling to hurricane wave overtopping and inundation. Ocean Engineering 37(1), 135-153.

McCall, R., Van Thiel de Vries, J.S.M., Plant, N.G., Van Dongeren, A.R., Roelvink, J.A.,Thompson, D.M., Reniers, A.J.H.M., 2010. Two-dimensional time dependent hurricane overwash and erosion modeling at Santa Rosa Island. Coastal Engineering 57, 668683.

McCall, R. 2013. XBeach Forum, Available at: `http://oss.deltares.nl/web/xbeach/forum/-/message_boards/view_message/230649`

Mawdsley, R.J., Haigh, I.D., Wells, N.C., 2015. Global secular changes in different high water, low water and range levels. Earth's Future, 3, 66-81.

Martinelli, L., Zanuttigh, B., Corbau, C., 2010. Assessment of coastal flooding hazard along the Emilia Romagna littoral, IT. Coastal Engineering 57, 1042-1058.

Nicholls, R.J., 2010. Impacts of and responses to sea-level rise in: Understanding Sea-Level Rise and Variability. Eds J.A. Church, P.L. Woodworth, T. Aarup, and W.W. Wilson, Wiley-Blackwell, Chichester, UK.

National Oceanic and Atmospheric Adminstation (NOAA). Sea Level Rise and Coastal Flooding Impacts. Accessed May 5, 2015 at http://coast.noaa.gov/slr/.

Poulter, B. and Halpin, P.N., 2008. Raster modelling of coastal flooding from sea-level rise. International Journal of Geographical Information Science 22(2), 167-182.

Prime T., Brown J.M., Plater A.J., 2015. Physical and Economic Impacts of Sea-Level Rise and Low Probability Flooding Events on Coastal Communities. PLoS ONE 10(2): e0117030. doi:10.1371/journal.pone.0117030

Pullen, T., Allsop, N.W.H., Bruce, T., Kortenhaus, A., Schüttrumpf H., Van der Meer, J.W., 2007. EurOtop: Wave overtopping of sea defences and related structures: Assessment manual. Available at http://www.overtopping-manual.com/manual.html.

Purvis, M.J., Bates, P.D., Hayes, C.M., 2008. A probabilistic methodology to simulate future coastal flood risk due to sea level rise. Coastal Engineering 55, 1062-1073.

Reeve, D.E., Soliman, A., Lin, P.Z., 2008. Numerical study of combined overflow and wave overtopping over a smooth impermeable seawall. Coastal Engineering 55, 155-166.

Roelvink, D., Reniers, A., Van Dongeren, A., van Thiel de Vries, J., McCall, R., Lescinski, J. 2009. Modelling storm impacts on beaches, dunes and barrier islands. Coastal Engineering, 56, 1133-1152.

Sanders, B.F., 2007. Evaluation of on-line DEMs for flood inundation modeling. Advances in Water Resources 30(8), 1831-1843.

Shewchuk, J.R., 1996. Triangle: engineering a 2D quality mesh generator and Delaunay triangulator in: Applied computational geometry: towards geometric engineering. in: Lin M.C., Manocha D., (Eds). Lecture Notes in Computer Science, vol 1148. Springer-Verlag, p. 203-222. Software: <http://www-2.cs/cmu.edu/˜quake/triangle.html>

Smit, P., Stelling, G., Roelvink, J.A., Van Thiel de Vries, J.S.M., McCall, R.T., Van Dongeren, A.R., Zwinkels, C. and R. Jacobs, 2010. XBeach: Non-hydrostatic model: Validation, verification and model description. Technical report, Delft University of Technology.

Smith, R.A.E. Bates, P.D., Hayes, C., 2012. Evaluation of a coastal flood inundation model using hard and soft data. Environmental Modelling and Software, 30, 35-46.

Splinter, K.D. and Palmsten, M.L., 2012. Modeling dune response to an east coast low. Mar. Geol. 329331, 4657.

Stockdon, H.F., Holman, R.A., Howd, P.A., Sallenger, A.H., 2006. Empirical parameterization of setup, swash and runup. Coastal Engineering 53, 573-588.

Stockdon, H.F., Thompson, D.M., Plant, N.G., Long J.W., 2014. Evaluation of wave runup predictions from numerical and parametric models. Coastal Engineering, 92, 1-11.

Sweet, W.V. and Park, J., 2014. From the extreme to the mean: Acceleration and tipping points of coastal inundation from sea level rise. Earth's Future, 2, 1-11.

Taylor, Peter J., 1977. Quantitative Methods in Geography: An Introduction to Spatial Analysis. Boston, Massachusetts: Houghton Mifflin Harcourt, 396 p.

TAW, 2002. Technical report wave run-up and wave overtopping at dikes,Technical Advisory Committee on Flood Defence, The Netherlands.

Tebaldi, C., Strauss, B.H., Zervas, C.E., 2012. Modelling sea level rise impacts on storm surges along US coasts. Environmental Research Letters 7, 12 pp.

Tsubaki, R., Fujita, I., 2010. Unstructured grid generation using LiDAR data for urban flood inundation modeling. Hydrological Processes 24, 14041420.

Wadey, M.P., Nicholls, R.J., Hutton, C., 2012. Coastal Flooding in the Solent: An Integrated Analysis of Defences and Inundation. Water, 4, 430-459.

Zijlema, M. and G. S. Stelling, 2008. Efficient computation of surf zone waves using the nonlinear shallow water equations with non-hydrostatic pressure. Coastal Engineering 55(10), 780-790.

Figure 1: Imperial Beach Site and Data Sources. (A) Bathymetry with XBeach transects envelope (striped area) and 10-40m isobaths. (B) nearshore data with 10 m isobath. Xbeach transects 3, 6 and 9 are shown as solid blue, red and green lines, respectively. Inset C: Flood modeling domain, transects and observed flood extent (blue). (D) Foreshore transects, black arrows denote slope toes. Numerals correspond to geospatial data priorities in Table 1. All data in NAVD88 m unless otherwise shown.

Figure 2: Site Specific Topography. (A) Google Earth back beach topography showing terrain features between houses. (B) LiDAR DSM and bare earth DEM comparison along a transect between structures where bare earth DEM is oversmoothed.

Figure 3: Wave and water level data. (A) offshore peak period, (B) peak direction, (C) significant wave height, (D) water level (black line) and TWL estimates for $R_2\%$ runup ($*$) and setup ($+$). Transect colors as described in Figure 1. Grey band shows minimum and maximum beach crest.

Figure 4: (A) SWAN significant wave height output at 1600 UTC with XBeach transect envelope (striped area) and 10-40 m isobaths (B) XBeach 40 m boundary, nonhydrostatic water level (blue) at 1600 UTC along transect 6. Inset (C) Beach detail, arrow shows nearshore overtopping estimate location.

Figure 5: Summary of all XBeach overtopping realizations for each transect. 10 m boundary (white background, dashed lines), 40 m boundary (grey background, solid lines), hydrostatic (blue bars), nonhydrostatic (red bars). Realization mean is shown by circle and cross, vertical bars represent minimum and maximum of 10 runs. Asterisk are used when 80% or more of

realizations predicted zero overtopping).

Figure 6: Dynamic overtopping rates for (A) EurOtop, (B) 10 m XBeach, (C) 40 m XBeach and (D) cumulative total overtopped volume.

Figure 7: Static (A) Stockdon R_2% TWL and dynamic (B) EurOtop, (C) 10 m XBeach, (D) 40 m XBeach flood predictions and field validation data (black line). Stockdon setup predicted no flooding and is not shown. Static models do not predict flooding depth, extent is shown in red.

Figure 1

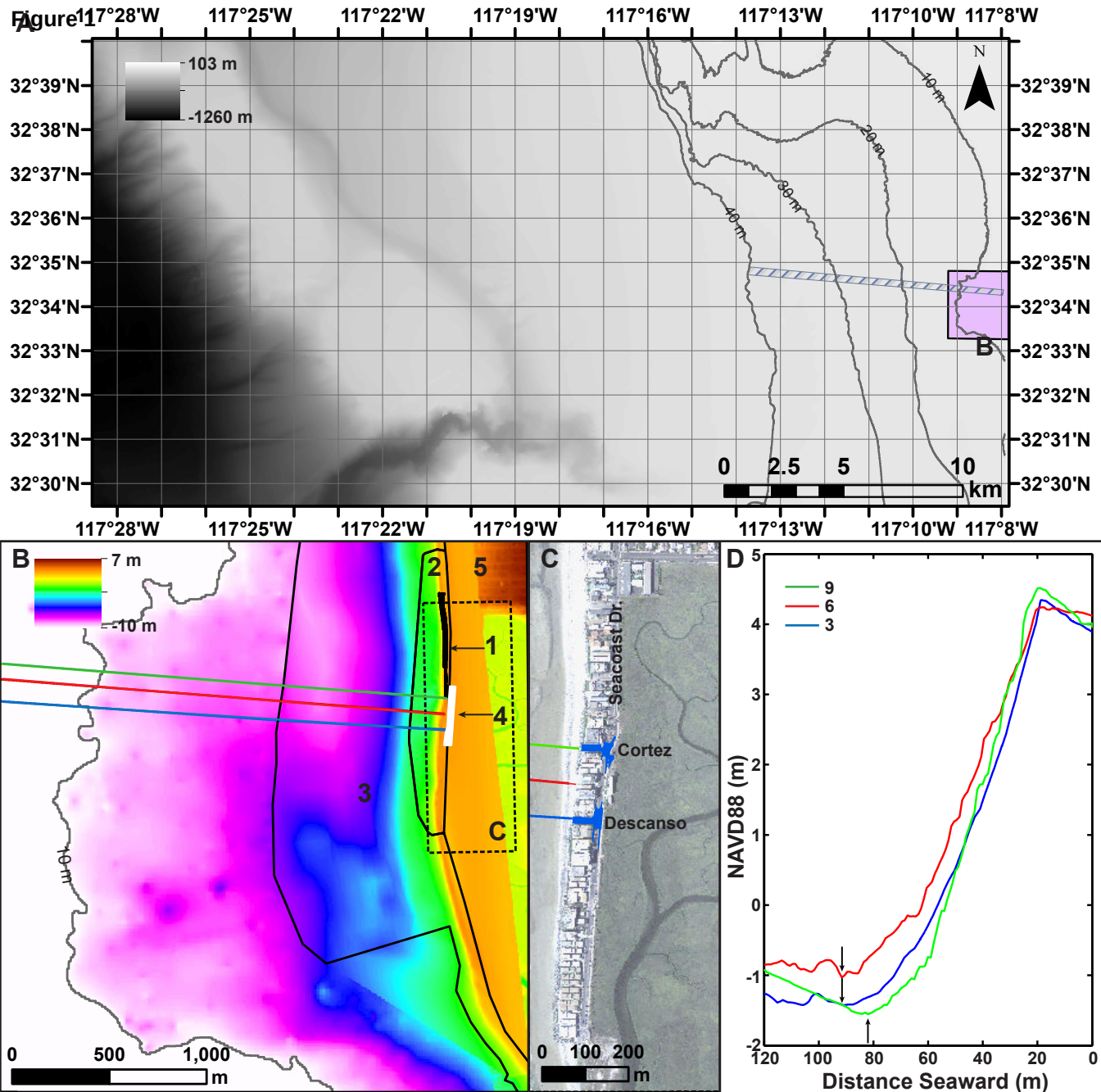
A
117°28'W
117°25'W
117°22'W
117°19'W
117°16'W
117°13'W
117°10'W
117°8'W
32°39'N
32°38'N
32°37'N
32°36'N
32°35'N
32°34'N
32°33'N
32°32'N
32°31'N
32°30'N
103 m
-1260 m
10 m
20 m
30 m
40 m
N
B
0 2.5 5 10
km
B
7 m
-10 m
1
2
3
4
5
C
10 m
0 500 1,000
m
C
Seacoast Dr.
Cortez
Descanso
0 100 200
m
D
9
6
3
NAVD88 (m)
Distance Seaward (m)
120 100 80 60 40 20 0
5 4 3 2 1 0 -1 -2

Figure 2


A
Lawn
Footpath
Stairs
Street

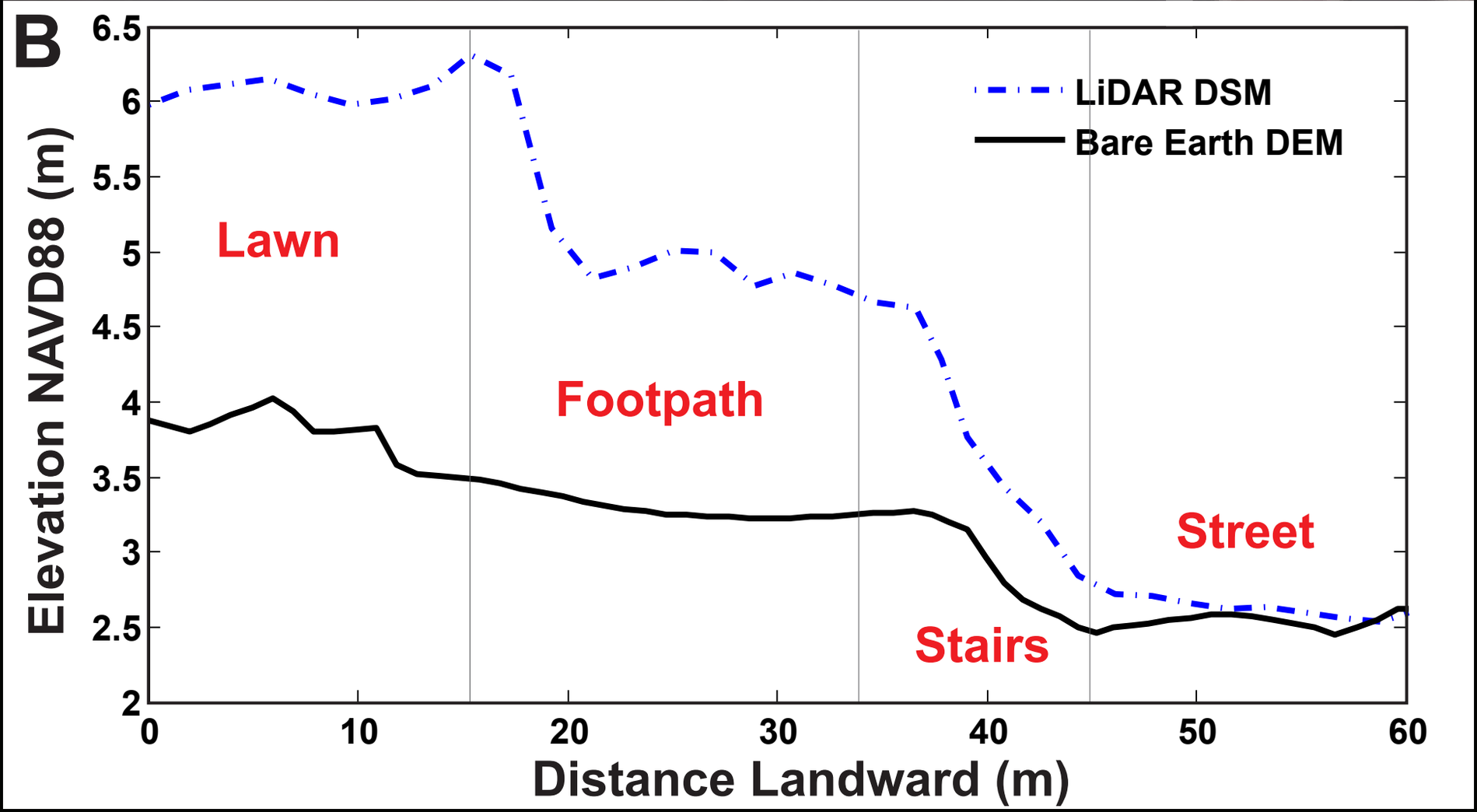
B
LiDAR DSM
Bare Earth DEM
Lawn
Footpath
Street
Stairs
Elevation NAVD88 (m)
Distance Landward (m)
6.5
6
5.5
5
4.5
4
3.5
3
2.5
2
0
10
20
30
40
50
60

Figure 3

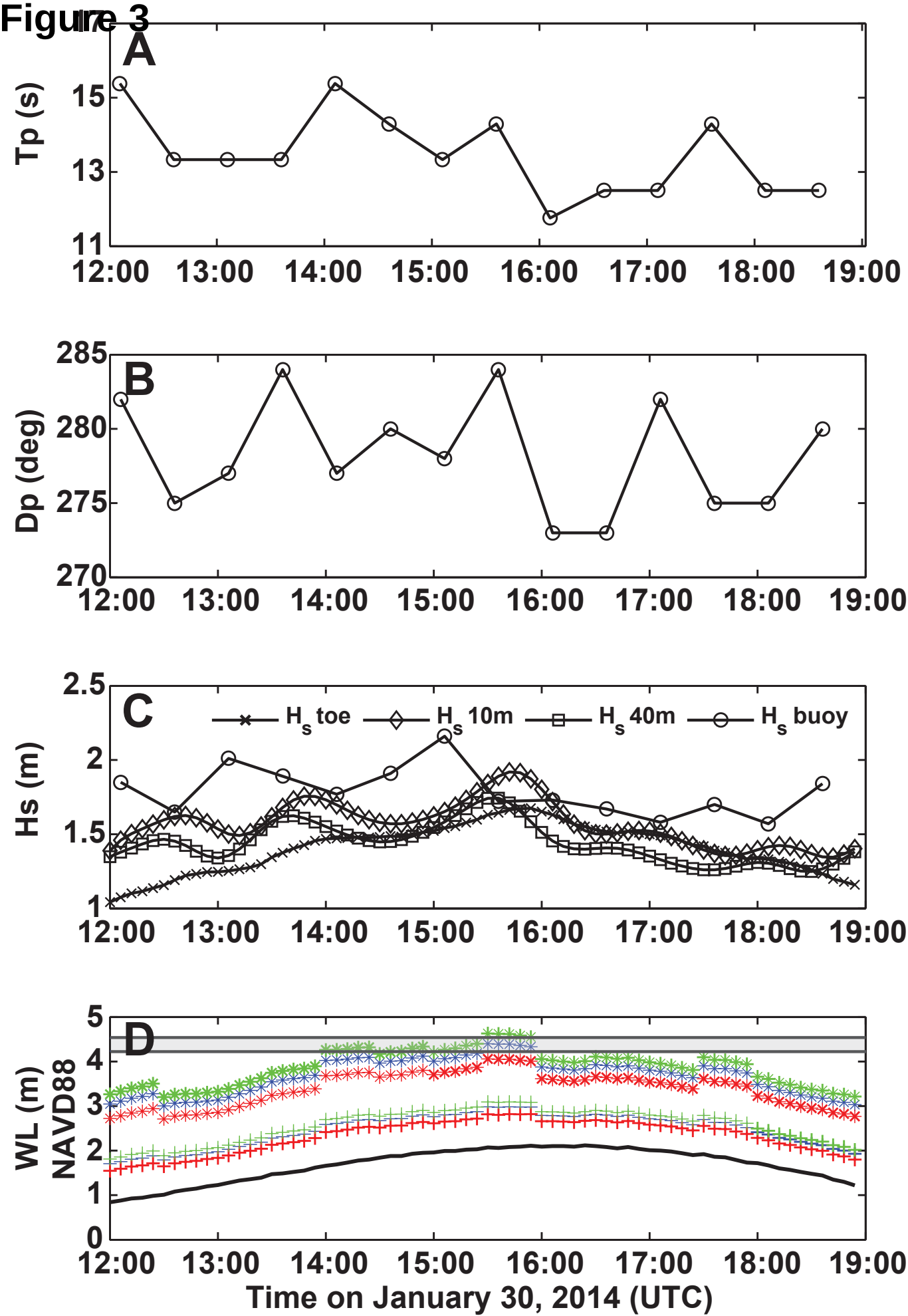
A
Tp (s)
15
13
11
12:00
13:00
14:00
15:00
16:00
17:00
18:00
19:00
B
Dp (deg)
285
280
275
270
C
Hs (m)
2.5
2
1.5
1
H_s toe
H_s 10m
H_s 40m
H_s buoy
D
WL (m)
NAVD88
5
4
3
2
1
0
Time on January 30, 2014 (UTC)

Figure 14

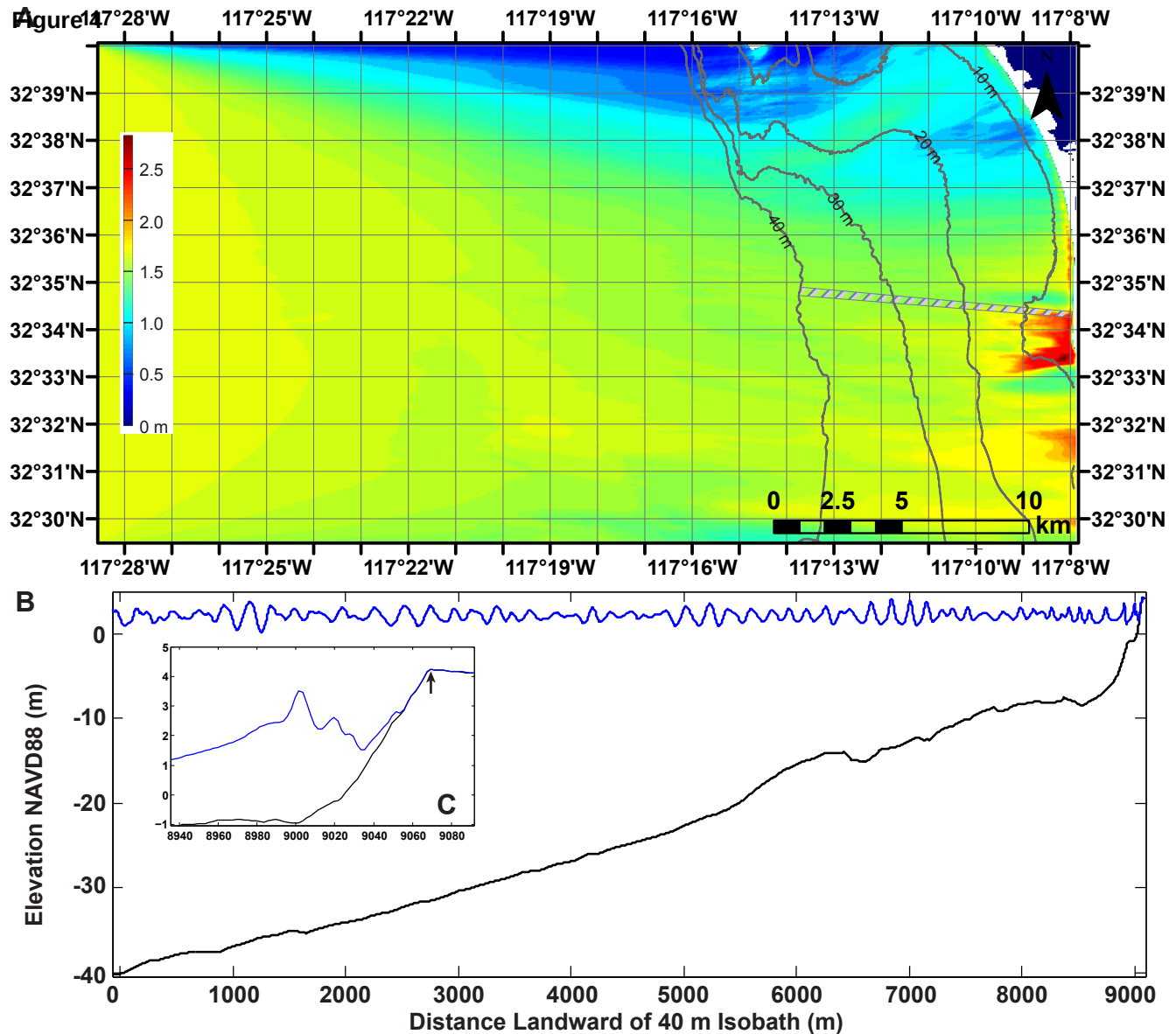
A
117°28'W
117°25'W
117°22'W
117°19'W
117°16'W
117°13'W
117°10'W
117°8'W
32°39'N
32°38'N
32°37'N
32°36'N
32°35'N
32°34'N
32°33'N
32°32'N
32°31'N
32°30'N
2.5
2.0
1.5
1.0
0.5
0 m
10 m
20 m
30 m
40 m
N
0
2.5
5
10
km
B
Elevation NAVD88 (m)
0
-10
-20
-30
-40
0
1000
2000
3000
4000
5000
6000
7000
8000
9000
Distance Landward of 40 m Isobath (m)
C
8940
8960
8980
9000
9020
9040
9060
9080

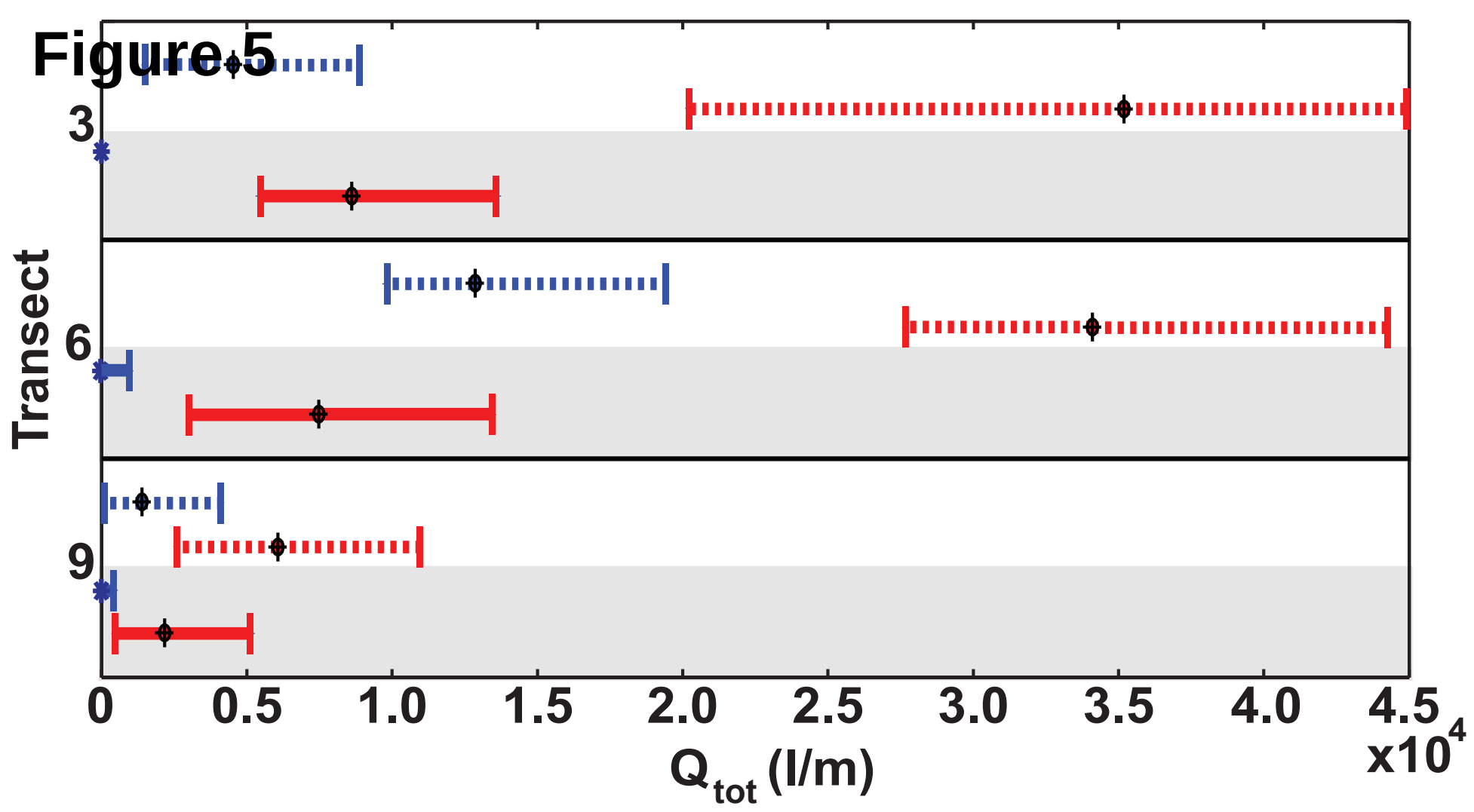
Figure 5
Transect
3
6
9
0
0.5
1.0
1.5
2.0
2.5
3.0
3.5
4.0
4.5
x10^4
Q_tot (l/m)

Figure 6

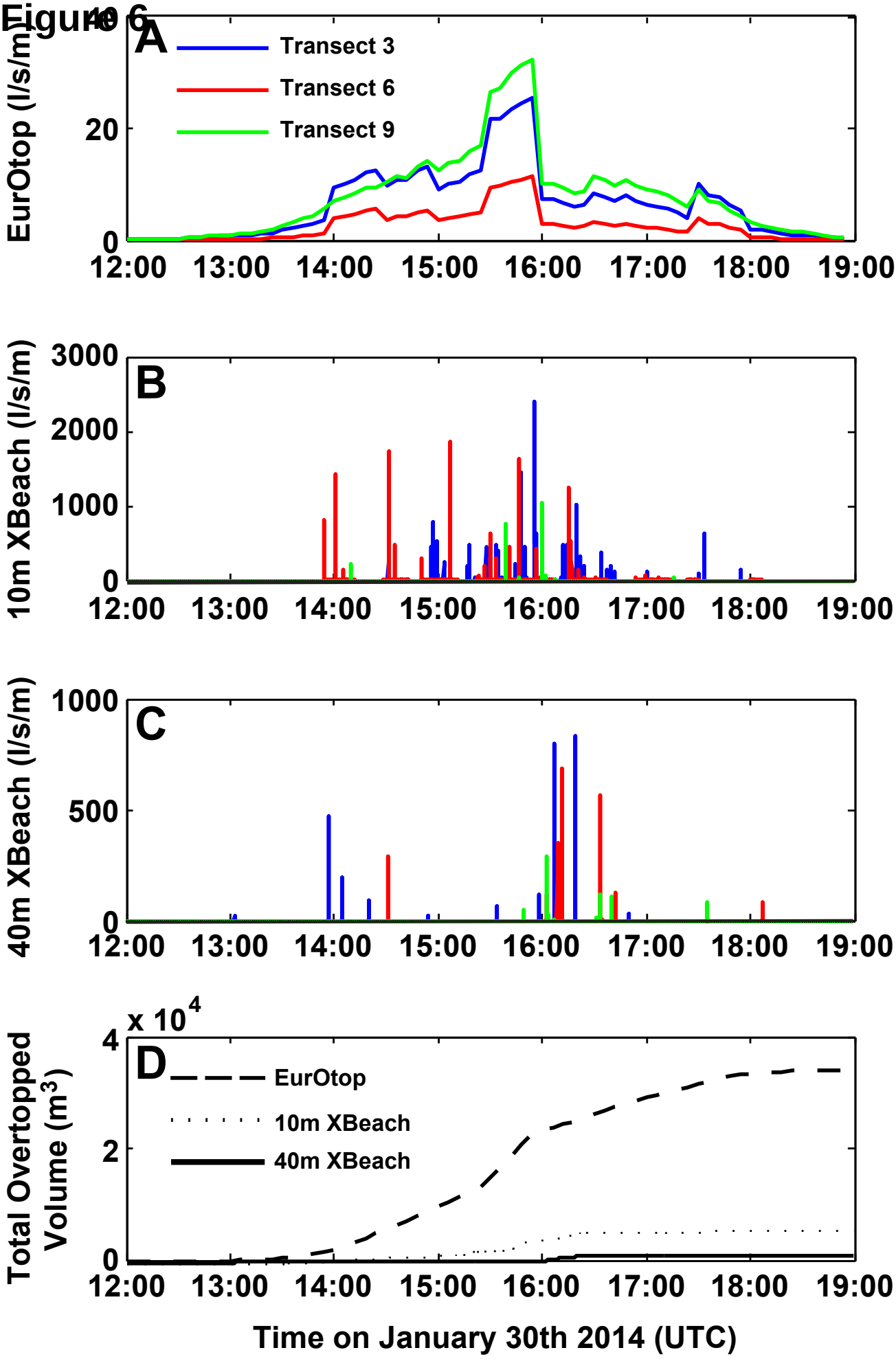
A
Transect 3
Transect 6
Transect 9
EurOtop (l/s/m)
40
20
0
12:00
13:00
14:00
15:00
16:00
17:00
18:00
19:00
B
10m XBeach (l/s/m)
3000
2000
1000
0
C
40m XBeach (l/s/m)
1000
500
0
D
x 10^4
Total Overtopped Volume (m^3)
4
2
0
EurOtop
10m XBeach
40m XBeach
Time on January 30th 2014 (UTC)

Figure 7

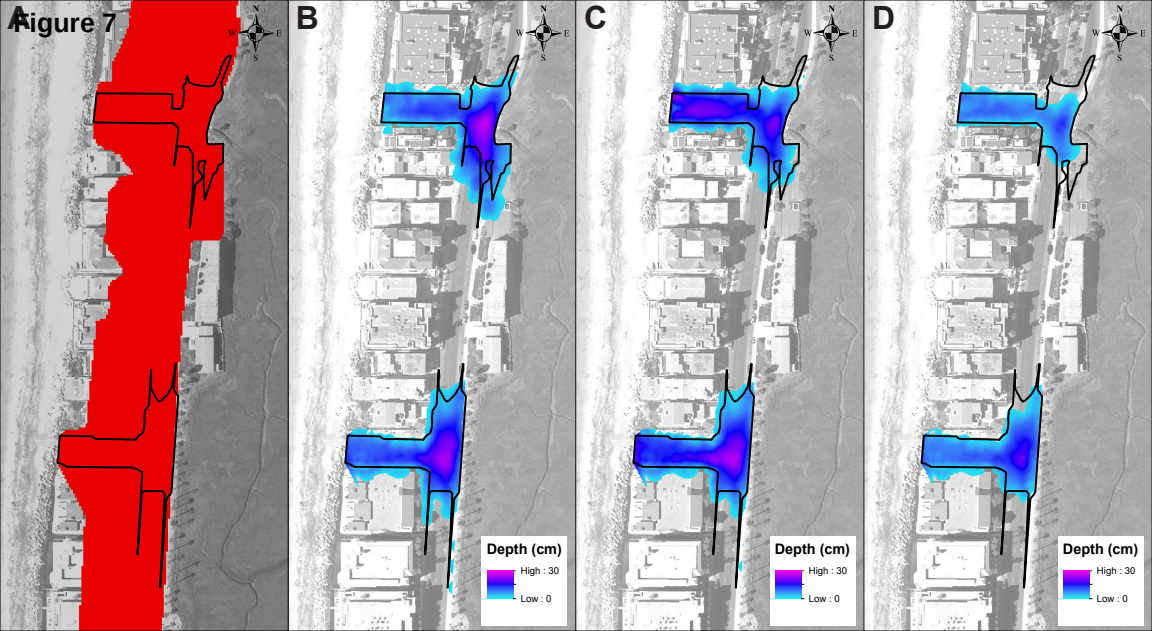

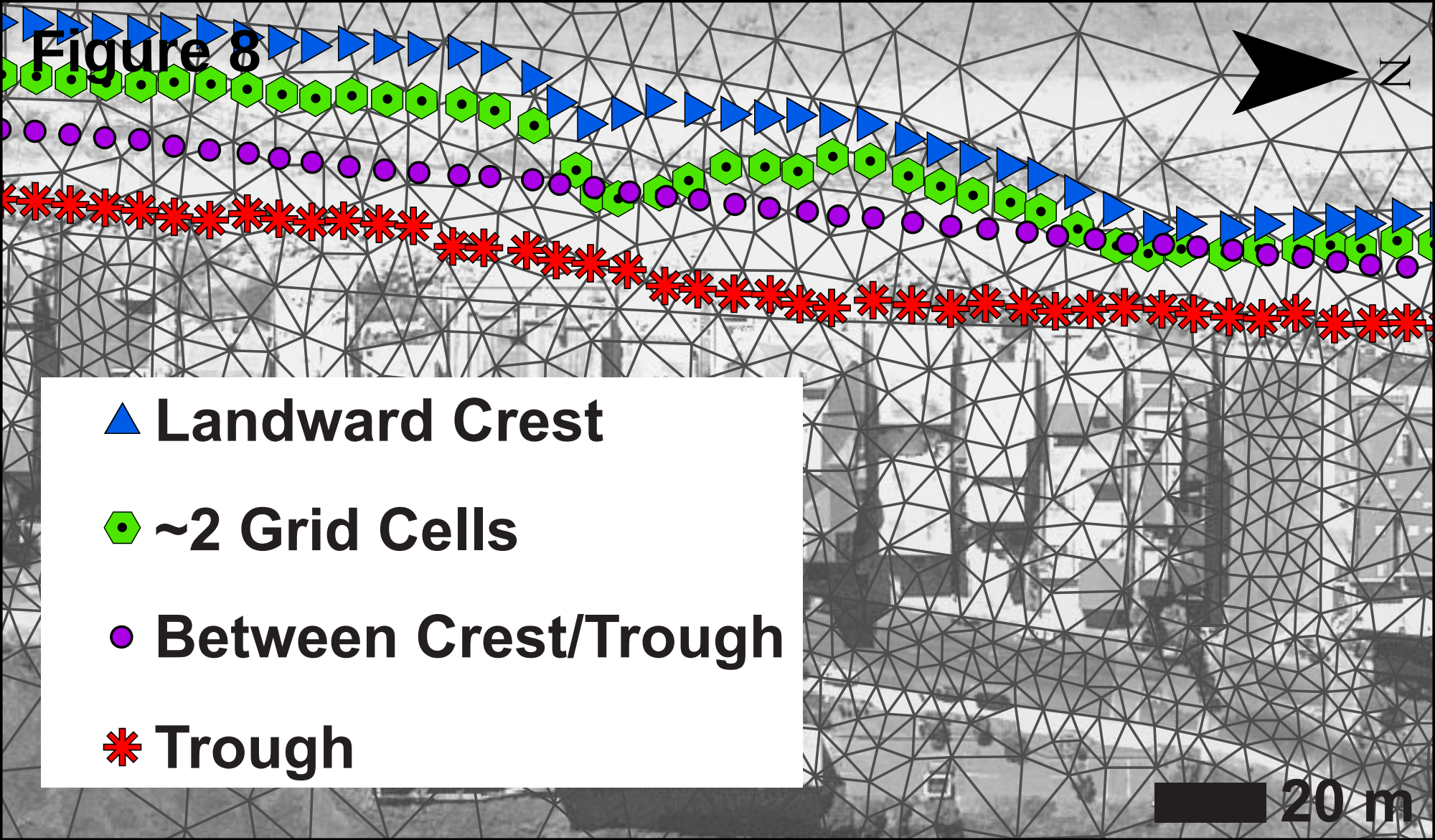
Figure 8
N
Landward Crest
~2 Grid Cells
Between Crest/Trough
Trough
20 m